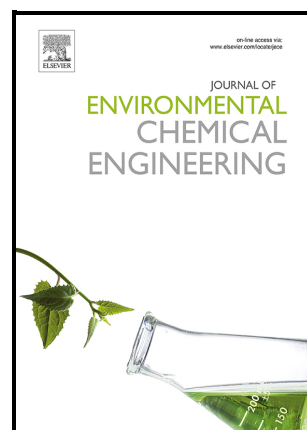


ROBUST SYSTEM FOR THE REGENERATIVE  
CAPTURE OF AQUEOUS POLLUTANTS  
WITH CONTINUOUSLY SYNTHESIZED AND  
FUNCTIONALIZED MAGNETIC  
NANOPARTICLES

Belén García-Merino, Eugenio Bringas, Inmaculada  
Ortiz-Uribe



PII: S2213-3437(22)01290-8

DOI: <https://doi.org/10.1016/j.jece.2022.108417>

Reference: JECE108417

To appear in: *Journal of Environmental Chemical Engineering*

Received date: 1 May 2022

Revised date: 2 August 2022

Accepted date: 8 August 2022

Please cite this article as: Belén García-Merino, Eugenio Bringas and Inmaculada Ortiz-Uribe, ROBUST SYSTEM FOR THE REGENERATIVE CAPTURE OF AQUEOUS POLLUTANTS WITH CONTINUOUSLY SYNTHESIZED AND FUNCTIONALIZED MAGNETIC NANOPARTICLES, *Journal of Environmental Chemical Engineering*, (2022) doi:<https://doi.org/10.1016/j.jece.2022.108417>

This is a PDF file of an article that has undergone enhancements after acceptance, such as the addition of a cover page and metadata, and formatting for readability, but it is not yet the definitive version of record. This version will undergo additional copyediting, typesetting and review before it is published in its final form, but we are providing this version to give early visibility of the article. Please note that, during the production process, errors may be discovered which could affect the content, and all legal disclaimers that apply to the journal pertain.

© 2022 Published by Elsevier.

# ROBUST SYSTEM FOR THE REGENERATIVE CAPTURE OF AQUEOUS POLLUTANTS WITH CONTINUOUSLY SYNTHESIZED AND FUNCTIONALIZED MAGNETIC NANOPARTICLES

Belén García-Merino, Eugenio Bringas and Inmaculada Ortiz-Uribe\*

Department of Chemical and Biomolecular Engineering, ETSIT, University of Cantabria, Avda. Los Castros s/n, 39005 Santander, Spain.

\*Corresponding author: Inmaculada Ortiz-Uribe, e-mail: ortizi@unican.es

## Abstract

Nowadays, the design of efficient technologies for the detection and separation of environmental pollutants from aqueous solutions continues to be a challenge to the industrial sector. The present work proposes a robust microfluidic system for the continuous, rapid and effective testing of selective capture agents of aqueous pollutants based on the use of magnetic nanoparticles, MNPs. These are found of special interest due to their high specific surface area, easy functionalization and superparamagnetic behavior. In this work, MNPs with an average diameter of  $8.8 \pm 1.3$  nm and amino-functionalization were obtained following a novel continuous synthesis that facilitated the control of the particles properties. The microfluidic capture of Cr(VI) from aqueous solutions was assessed as representative case study; followed by the successful regeneration of loaded MNPs. The obtained results prove the advantages of the proposed system: i) continuous synthesis of functionalized MNPs with rigorous size control, ii) selective and fast capture of the target compound depending on the particle's functionalization and large surface area, respectively, iii) continuous operation that facilitates process scale-up, iv) easy regeneration of the functional materials, and v) magnetic separation of MNPs from fluid media if needed. Furthermore, the calculated Cr(VI) maximum uptake is higher than obtained values for non-functionalized MNPs and is in the range of previously reported data for ion exchange resins, with the additional advantages already mentioned. Thus, this work constitutes a step forward in the methodological design of advanced systems for the detection or separation purposes and can be extended to a wide variety of pollutants.

## Keywords:

continuous synthesis, functionalized magnetic nanoparticles (MNPs), aqueous pollutants, hexavalent chromium (Cr(VI)), microfluidic capture and regeneration.

## 1. Introduction

Nowadays, the detection and separation of persistent and emerging pollutants from wastewaters and effluents is considered a major challenge in the industrial sector. The present work contributes to the design of microfluidic systems for the continuous and controllable synthesis of functionalized magnetic nanoparticles (MNPs), followed by the rapid and effective capture of aqueous pollutants and the regeneration of the pollutant loaded particles. Thus, we report the experimental assessment of a microfluidic platform that could be used in the screening of the performance of new materials for environmental remediation of polluted waters. Magnetic nanomaterials include particles composed of pure iron, nickel, cobalt and their oxides, ferrites and metallic alloys. These nanoparticles are considered of special interest for their use in solid-liquid separations due to their unique properties including i) high loading capacity which favors the interaction with target compounds, ii) easy functionalization capacity which gives selectivity to the interaction, iii) chemical stability, iv) low intraparticulate diffusion rate and, v)

superparamagnetic behavior for particles below a certain diameter which is material-dependent. Superparamagnetism is a phenomenon that causes a strong response to an external field and enables the separation of the particles from complex multiphase systems under the action of a magnetic field. Superparamagnetic materials show high values of magnetic saturation, several orders of magnitude greater than the usual values for paramagnetic materials. In addition, their magnetic properties are lost when the external field is removed, as the coercivity value is zero; therefore, they do not attract each other, reducing the risk of agglomeration when used in different applications[1–3]. The use of MNPs is of great importance in environmental applications, where functional groups can enhance the selectivity of MNPs for their use as magnetic sensors to detect harmful substances and as adsorbents for the selective capture of pollutants. MNPs show high mobility, resulting in short diffusion distances, lower doses and faster kinetics compared to other conventional adsorbents, which reduce operating costs and increase efficiency [4–6].

This work reports a methodology for the continuous synthesis and functionalization of selective MNPs, and for their application to the microfluidic capture of aqueous pollutants. To this end, the capture of Cr(VI) present in aqueous solutions using amine functionalized MNPs has been chosen as representative case study. This model system was selected because it has been widely studied in the literature working with two liquid phases or with conventional solid-liquid separations [7–15]. In recent works, the use of magnetic composites [16,17] or magnetic nanoparticles [18–21] as adsorbents for the capture of Cr(VI) has been taken into consideration, showing the advantages of these materials for the said application. Here, we advance previous knowledge by the analysis of the process from a holistic point of view. The maximum capture capacity of functionalized MNPs was initially determined from equilibrium experiments and compared with available data of commercial ion exchange resins. Then, the microfluidic regeneration of the loaded particles was studied, as well as their possible reusability in the capture stage. Fluid flow in microdevices is under the laminar regime with small residence times; additionally, microdevices offer a high area/volume ratio, improved mass and heat transfer kinetics and the possibility to work within a continuous mode. Besides, they can be designed with different geometries, enhancing mixing of the reactants and preventing MNPs agglomeration and adhesion to the walls. Microfluidic devices are suitable for the study of environmental magnetic separations and are an excellent example of process intensification, allowing the continuous capture and separation of the target compounds in continuous operation mode. The functionalized MNPs are injected into the microdevice and key compounds with acceptable affinity for the functionalized surface are captured through specific ligand-receptor binding, without affecting the rest of the fluid components. Loaded MNPs can be separated from the fluid by means of magnetic gradients, easily regenerated and reused [22–24].

For the successful achievement of the pollutants capture, MNPs must provide efficient removal of the target compounds, being selectivity and capture rate key parameters that usually face a tedious process in the synthesis and functionalization steps of the particles. This remarks the need to find alternatives for the production of functionalized MNPs, which allow a proper control of size, shape, crystal structure and surface modification to adapt the synthesized particles to the requirements of the target application. This may include reducing agglomeration and water insolubility, preventing oxidation and corrosion in ambient conditions, and providing selectivity to the capture thanks to the anchored functional groups. The mostly applied conventional approaches for the synthesis of MNPs are the chemical routes, also called bottom-up strategies, specially coprecipitation and thermal decomposition. The first one, is a simple, cheap, efficient, and well-characterized method, whereas the second one enables the separation of MNPs nucleation and growth steps, allowing higher control of particles size. In this work, these two alternatives have been studied and compared, as well as the most recent strategy, the implementation of a microdevice in the MNPs synthesis, to take advantage of the previously

described benefits of microfluidics [25–27]. In addition, a post-synthesis functionalization is applied in a second step, in which an aminoalcosixilane is used to provide primary and secondary amino groups for their anchorage in the magnetic particles surface. This amino-functionalization has been largely considered in literature, showing a high capacity to capture a wide range of metals in anionic form [28,29]. The functionalization step has been developed in this study both in batch mode and within the use of a microdevice, for comparison.

## 2. MATERIALS AND METHODS

### 2.1 Reactants and microfluidic device

All chemicals were used as received without further purification and all solutions were prepared with ultrapure water (18 MΩcm, MilliQ, Milipore). Triethylene glycol (TEG,  $C_6H_{14}O_4$ ) and ethyl acetate ( $C_4H_8O_2$ , 99.9%) were obtained by Fisher Chemical. Iron (III) acetylacetonate ( $Fe(acac)_3$ , 97%), ferrous chloride ( $FeCl_2 \cdot 4H_2O$ , ≥99%), ferric chloride ( $FeCl_3 \cdot 6H_2O$ , ≥99%), N-[3-(Trimethoxysilyl)propyl] ethylenediamine (TMPEd, 99%) and hydrochloric acid (HCl, 2M, 37%) were purchased by Sigma-aldrich. Sodium hydroxide (NaOH, 1M), toluene dry ( $C_6H_5CH_3$ , 99%) and iso-propyl alcohol ( $C_3H_8O$ , 99.5%) were supplied by PanReac AppliChem. Ethanol ( $C_2H_5OH$ , ≥99.5%) was obtained from Merck and finally, potassium chromate ( $K_2CrO_4$ ) was provided by Scharlau. The microdevice used for the continuous experiments, including synthesis, functionalization, Cr(VI) capture and MNPs regeneration, is shown in Figure 1. It is a spiral shape microreactor made of polymeric resin using a ultimaker s3 3D printer, with two inlets, one outlet, 400mm longitude and a circular section of 3mm diameter. Tetrafluoroethylene tubing (0.3mm ID and 1.58mm OD) was employed to connect the microdevice with a pressure pump (Asia Flow Chemistry Syringe Pump, Syrris).

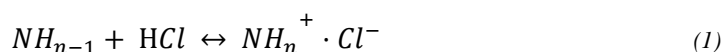
### 2.2 MNPs synthesis and functionalization

In this work, two MNPs synthesis methods have been followed, thermal decomposition and coprecipitation, to test the influence of the process in the particle's characteristics including size, shape and agglomeration effects. The synthesis has been followed by a functionalization step to convert the magnetic cores into smart systems viable for the desired application. The last attempt has been to implement the use of microfluidics in both the synthesis and functionalization steps, to achieve a continuous and more controllable production of surface-modified MNPs. The different approaches and their combinations are summarized in Table 1.

The batch thermal decomposition synthesis (BTD) is based on a procedure previously reported by Cai and Wan [30]. This way, 75ml of TEG and 2.12g of  $Fe(acac)_3$  were sonicated for 5min (FB 15050, Fisher Scientific) and poured into a three-neck round-bottom flask equipped with condenser, magnetic stirrer, heating mantle and nitrogen inlet to obtain an inert atmosphere. Later, the mixture was heated until it reached 180°C, kept there for 30min and heated to 280°C for another 30min. The resulting suspension was cooled down to room temperature and particles, consisting of a magnetite core and a TEG coating, were centrifuged (Eppendorf 5810) and separated with the help of a magnet. Then, MNPs were purified three times with 30ml of ethanol and 60ml of ethyl acetate, to remove the excess of TEG and other by-products, and left in the oven at 100°C until they were completely dry. For the batch coprecipitation method (BC), 50 mL of a 0.57M NaOH solution and 50mL of a 0.1M Fe solution, prepared with 1:2  $FeCl_2 \cdot 4H_2O$ :  $FeCl_3 \cdot 6H_2O$  molar ratio, were mixed in a three-neck round-bottom flask with magnetic stirrer and nitrogen inlet, for 30min at 60°C, using a heating mantle. The resulting suspension was cooled down to room temperature and particles were centrifuged and separated with the help of a magnet. Then, MNPs were purified three times with 30ml of ethanol and left in the oven at 100°C until they were completely dry. The experimental setup for the continuous

coprecipitation method (CC) is shown in Figure 1A. In this case, 0.1M Fe solution and 0.57M NaOH solution were introduced in the previously described microdevice, which was submerged in a thermal bath at 60°C. The total residence time of the MNPs inside the microreactor was 2min 40s, selected based on previous studies by Besenhard et al [31], in which the total residence time for a continuous coprecipitation synthesis of MNPs with NaOH was <5min. The MNPs were collected at the outlet, centrifuged, separated from the rest of solution with the help of a magnet, purified with ethanol and dried.

The functionalization was applied to anchor primary and secondary amino groups on the surface of the MNPs, which apart from reducing their tendency to agglomerate, allow the protonation of the particles for their use as ion exchangers in the Cr(VI) capture process. The amino functional groups are incorporated in the particles by means of the aminoalcoxysilane TMPED. In the case of batch functionalization (BF), 2mL of TMPED, 500mg of nanoparticles and 50ml of toluene were sonicated for 5 minutes, poured into a three-neck round-bottom flask and heated with a heating mantle to 110°C for 3h, under stirring, with reflux and an inert nitrogen atmosphere. The resulting suspension was cooled down at room temperature and centrifuged, then the particles were separated with the help of a magnet, cleaned three times with 10 mL of iso-propyl alcohol and dried in the oven at 120°C to eliminate traces of toluene. For the continuous functionalization (CF), a suspension of  $5000\text{mg}_{\text{MNPs}} \cdot \text{L}^{-1}$  of MNPs and a solution of  $9 \cdot 10^{-2}\text{M}$  of TMPED in ultrapure water were introduced in the previously described microreactor at ambient temperature with 4min of residence time. Functionalized MNPs are collected at the outlet, the solution is centrifuged and particles are separated from the rest of the supernatant liquid with the help of a magnet, purified with iso-propyl alcohol and dried. Finally, to achieve the capture of Cr(VI) by means of ion exchange, amino-functionalized MNPs must be protonated with an inorganic acid. To this end, a solution of 0.01M HCl was added to the particles with a ratio of  $500\text{mL} \cdot \text{g}_{\text{particle}}^{-1}$ . The suspension was sonicated for 5min and left under stirring for 6h at room temperature, thus, reaction between chloridric acid and primary and secondary amino groups takes place according to Equation 1. The resulting solution was centrifuged, magnetized to separate the particles, cleaned three times with UP water and placed in the oven at 100°C until the particles were completely dry.



### 2.3 MNPs characterization

To verify the correct synthesis and functionalization of the magnetite particles and their feasibility for Cr(VI) uptake, several characterization methods were applied. First, Fourier-transform infrared spectroscopy (FT-IR) was performed with a spectrum 65 spectrometer Perkin Elmer equipment. The measurement was carried out in a reflectance spectrum between 400 and 4000 $\text{cm}^{-1}$ , with a resolution of  $4\text{cm}^{-1}$ , 150scans and a step speed of  $2\text{mm} \cdot \text{s}^{-1}$ . X ray diffraction spectra were obtained using a Bruker D8 Advance equipment, equipped with a copper tube ( $\langle \lambda \rangle = 1.542 \text{ \AA}$ ). The spectrum was collected at angles  $2\theta$  between 15-70° ( $\Delta 2\theta = 0,05^\circ$ ) at ambient temperature. The results obtained were analyzed by direct comparison with the diffraction pattern database in the International Centre for Diffraction Data (ICDD, PDF2). Zeta potential was analyzed by means of dynamic lights scattering techniques in a Zetasizer Nano ZS (Malvern) equipment. The equipment was calibrated with latex particles as reference material (DTS1235 standard) and all the measurements were carried out in triplicate, at room temperature, using  $0.1\text{mg} \cdot \text{mL}^{-1}$  solutions previously sonicated for 10min, with glass cuvettes of 17°C angle. The size and shape of the MNPs were determined in a Transmission Electron Microscope (TEM) Jeol JEM 1011 and a jeol JEM 2100; the obtained images were then studied using the software ImageJ. The magnetization curves of the particles were obtained with a Superconducting Quantum Interference Device (SQUID) magnetometer. A thermogravimetric analysis (TGA) was carried out in a TGA/DTA-DTG Shimadzu equipment, heating the sample

up to 1000 °C. The grafting density ( $\sigma_{TGA}$ ), number of bound molecules of aminoalcoxisilane per unit surface area, was estimated by applying Equation 2 [32–34], where  $W$  is the mass loss due to functional groups when a temperature of 1000°C is applied in the TGA analysis;  $\rho_o$ ,  $V_o$  and  $A_o$  correspond to the non-functionalized particles density ( $\text{g}\cdot\text{nm}^{-3}$ ), volume ( $\text{nm}^3$ ), and area ( $\text{nm}^2$ ) respectively;  $N_A$  is the Avogadro number ( $\text{molecules}\cdot\text{mol}^{-1}$ ) and  $M_w$  the molecular weight of the functional groups ( $\text{g}\cdot\text{mol}^{-1}$ ).

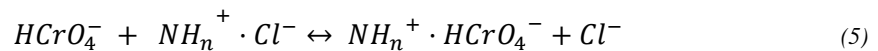
$$\sigma_{TGA} (\text{molecules} \cdot \text{nm}^{-2}) = \frac{\frac{W}{100-W} \rho_o \cdot V_o \cdot N_A}{M_w \cdot A_o} \quad (2)$$

The Brunauer-Emmett-Teller (BET) analysis was performed with a Tristar II Plus equipment, in order to calculate the specific area of the particles ( $S_a$ ,  $\text{m}^2\cdot\text{g}^{-1}$ ). Then, the functionalization degree of the MNPs (FD), which is given by the number of moles of the amino group per gram of particle, was estimated using Equation 3.

$$FD (\text{mol}_{NH_2} \cdot \text{g}_{MNPs}^{-1}) = \sigma_{TGA} \cdot S_a \cdot N_a \quad (3)$$

#### 2.4 Cr (VI) capture experiments

Several experiments were performed at room temperature to assess the performance of the functionalized particles on the capture of Cr(VI) anions, working both in batch mode and using the previously mentioned microfluidic device, as shown in Figure 1B<sub>1</sub>. In both batch and continuous experiments, a Cr(VI) solution of  $23\text{mg}\cdot\text{L}^{-1}$  was contacted with several suspensions of BTD-BF particles in the range  $2.5\text{-}72\text{g}_{MNPs}\cdot\text{L}^{-1}$ , to analyze the optimal conditions for a complete Cr(VI) uptake. In batch experiments, the contact between the liquid solution and MNPs took place in a falcon tube which was sonicated for 18min, selected as the optimal sonication time to ensure the complete deagglomeration of the particles, and therefore, the maximum active surface area for the capture of the target compound. In the continuous experiments, the contact took place in the microdevice working with a residence time of 18min, which means that  $78.5\mu\text{L}\cdot\text{min}^{-1}$  were circulated through each inlet of the microdevice; that time was selected to ensure the maximum Cr(VI) uptake for any value of MNPs concentration. In both cases, the mixture was centrifuged, particles were separated using a magnet and the supernatant was analyzed using microwave plasma atomic emission spectroscopy in an MP-AES Agilent spectrometer. In addition, the experiments were duplicated so that reproducibility could be proven, and the results are shown as mean values  $\pm$  standard deviation. The final pH of the experiments ranged between 6 when Cr(VI) was contacted with a  $2.5\text{g}_{MNPs}\cdot\text{L}^{-1}$  MNPs suspension, to pH 3.4 with a  $72\text{g}_{MNPs}\cdot\text{L}^{-1}$  MNPs suspension. At these pH values and for an initial Cr(VI) concentration of  $23\text{mg}\cdot\text{L}^{-1}$ , the Cr(VI) is present in the form of bichromate. The equilibrium reaction which gives place to bichromate anions is shown in Equation 4, which has an equilibrium constant of  $1.21\text{L}\cdot\text{mol}^{-1}$ [35]. This way, the mechanism of Cr(VI) removal takes place due to an ion exchange reaction between bichromate anions and primary and secondary protonated amino groups, as shown in Equation 5.



Using the data obtained from ICP analysis, the Cr(VI) capture percentages were determined by means of Equation 6, where  $C_{Cr(VI)}^i$  is the initial concentration of Cr(VI) in the problem solution ( $\text{mg}\cdot\text{L}^{-1}$ ),  $C_{Cr(VI)}^f$  is the final Cr(VI) concentration in solution ( $\text{mg}\cdot\text{L}^{-1}$ ) measured by ICP and  $V_i$  and  $V_f$  are the initial and final volumes of the aqueous solution (L).

$$Cr(VI) \text{ capture } (\%) = \frac{C_{Cr(VI)}^i \cdot V_i - C_{Cr(VI)}^f \cdot V_f}{C_{Cr(VI)}^i \cdot V_i} \cdot 100 \quad (6)$$

In addition, the Cr(VI) exchange capacity of the particles (EC) has been calculated for the different experimental conditions (MNPs suspension:  $2.5\text{-}72\text{g}_{\text{MNPs}}\cdot\text{L}^{-1}$ ) by means of Equation 7, where  $C_{\text{Cr(VI)}}^i$  is the initial concentration of Cr(VI) in the problem solution ( $\text{mg}\cdot\text{L}^{-1}$ ),  $C_{\text{Cr(VI)}}^f$  is the final Cr(VI) concentration in solution ( $\text{mg}\cdot\text{L}^{-1}$ ) measured by ICP and  $C_{\text{MNPs}}$  corresponds to the concentration of the MNPs suspension ( $\text{g}_{\text{MNPs}}\cdot\text{L}^{-1}$ ).

$$EC \left( \text{mg}_{\text{Cr(VI)}} \cdot \text{g}_{\text{MNPs}}^{-1} \right) = \frac{C_{\text{Cr(VI)}}^i - C_{\text{Cr(VI)}}^f}{C_{\text{MNPs}}} \quad (7)$$

Capture experiments were also performed with the CC-CF particles continuously synthesized and functionalized in this work, to calculate their maximum exchange capacity for its comparison with BTD-BF particles. The same was developed with CC particles, to compare the activity of bare magnetite adsorbents with the amino-functionalized MNPs proposed in this work. In both cases, it was applied the previously described protocol. Furthermore, a tailored experiment with an initial chromium concentration in the order of  $\mu\text{g}\cdot\text{L}^{-1}$  has been developed, to evaluate the viability of the proposed methodology for polluted waters with lower values of Cr(VI) concentration. To do so, a Cr(VI) solution of  $500\mu\text{g}\cdot\text{L}^{-1}$  was contacted with a  $0.28\text{g}_{\text{MNPs}}\cdot\text{L}^{-1}$  suspension, applying the previously reported methodology. Finally, the viability of the particles for their regeneration and further reuse was assessed. For the regeneration analysis, a second spiral shape microdevice was connected to the first capture stage as shown in Figure 1B<sub>2</sub>, and a 0.02M NaOH solution was introduced and remained inside the device 9min (residence time). The outlet mixture was centrifuged, particles were separated using a magnet and the supernatant liquid was analyzed using microwave plasma atomic emission spectroscopy. Afterwards, particles were protonated again with a 0.01M HCl solution and their reusability for the Cr(VI) capture was tested, applying the previously described protocols.

### 3. RESULTS AND DISCUSSION

#### 3.1 MNPs characterization

##### FTIR analysis

Figure 2 shows the Fourier-transform infrared spectrum of the different samples of MNPs. In all particles, iron oxide is the main material that conforms the core of the nanoparticles. Therefore, the spectra show an intense peak at  $560\text{cm}^{-1}$ , which corresponds to the characteristic absorption band of the Fe-O bond. Moreover, BTD and BTD-BF show peaks corresponding to O-H bending vibration, C-H bending and O-H stretching at wavelengths of  $1030$ ,  $1180\text{-}1450$  and  $1500\text{cm}^{-1}$  respectively, due to TEG molecules which form the coating of the iron oxide cores produced in the thermal decomposition synthesis [28,30,36,37]. Furthermore, after anchoring the amino-alkoxysilane, new peaks appear in the case of the BTD-BF, CC-BF and CC-CF samples, the stretching Si-O-Si and Fe-O-Si vibration at  $750\text{-}1200\text{cm}^{-1}$  corresponding to the siloxane groups, the C-H stretching vibrations at  $1300$  and  $2900\text{cm}^{-1}$  and the characteristic peaks of amine groups around  $1600\text{cm}^{-1}$  [28,37–39]. In view of the iron oxide peaks that appear in all the samples spectrum, it can be concluded that the particles had been successfully synthesized following both the batch and continuous coprecipitation method. The same particles but with a TEG coating were obtained when the batch thermal decomposition procedure was applied. Besides, the effective functionalization of the particles in batch mode, as well as in continuous mode, have been also confirmed due to the appearance of the peaks corresponding to the amino-alkoxysilane anchoring.

##### X-ray diffraction analysis

Fig 3 shows the normalized diffractograms of BTD and BC samples of nanoparticles as representative of the two synthesis methodologies studied in this work: thermal decomposition and coprecipitation. Both samples share the same peak profile, which corresponds to the main phase of a crystal structure and is compatible with nanostructured compounds. The position and intensity of the diffraction peaks, match with the magnetite database in the International Centre for Diffraction Data (ICDD, PDF2: 75-0449). The peaks position of the reference structure, together with the Miller indexes of the principal reflections have been included in Figure 3. Regarding BC sample, no additional peaks are observed, which means that there are no other phases present, remarking the high purity of the magnetite particles [31,40]. In the case of BTD sample, two additional reflections are observed around the angular positions  $2\theta = 24^\circ$  and  $2\theta = 26.5^\circ$ , which are not compatible with the main phase and therefore, could be indicative of a second minor phase. It can be related with other phases of pure iron oxides or hydroxides (hematite, maghemite, lepidocrocite, etc) or to other residual phases that may have appeared in the thermal decomposition synthesis process[30].

#### Zeta Potential

Figure 4 shows the values and trends of the zeta potential for all the samples, as a function of pH (from 2 to 12). Both bare and amino-functionalized MNPs are positively charged at acidic pH values and negatively charged at basic pH values. In the case of bare magnetite particles (BTD, BC and CC), the isoelectric point or point of zero charge is around pH 6, which is consistent with the values previously reported in literature [38,39,42,43]. After functionalization of the particles, the zeta potential moves to significantly higher positive values. This confirms the valuable presence of amino groups in the surface of the MNPs which promotes repulsion forces between the particles, considerably reducing their tendency to agglomerate. This change in their surface charge, also results in a shift of the isoelectric point to a higher value, around pH 8, as stated in literature [38,39], showing potentially viable particles to retain anionic compounds at  $\text{pH} < 8$ . In this work, the functionalized materials were contacted with a solution of 0.01M HCl, to protonate the amino groups anchored on the particles surface (Equation 1), resulting in a positive superficial charge. This way, the particles are expected to show high efficiency in the capture process of anionic Cr(VI) at acidic pH.

#### Particles size, shape and agglomeration

Figure 5 shows TEM images of the different particles. The BTD sample presents spherical shape with an average diameter of approximately 12nm. Similar results have been previously reported when the same thermal decomposition method was applied in the synthesis of MNPs. For example, an average diameter of 7nm was reported by Cai and Wan [30] and a diameter of 11nm by Maity et al [36]. In the case of particles synthesized following the coprecipitation method, they also present spherical shape but with slightly smaller diameters, in the range 8-9nm. The difference in size can be justified if we take into account the longer residence times applied in the thermal decomposition procedure. This, together with the TEG coating that is formed around the magnetite core, give place to bigger particles sizes. Moreover, comparing the samples BC and CC, narrower size distributions are observed when particles are synthesized in continuous mode, due to the higher control of flowrates and residence times. In addition, a notorious reduction of the agglomeration of the particles is appreciated, which can be attributed to the use of a microreactor with a spiral shape geometry that enhances mixing and reduces agglomeration and adhesion of the particles to the walls. These sizes are very similar to the values reported in literature following a continuous coprecipitation method by means of a

microdevice, for example, Suryawanshi et al [44] obtained diameters in the range 6.3-9.8nm and Besenhard et al [31] achieved a 7.5nm size. In addition, the samples BTD-BF, CC-BF and CC-CF present particles after their functionalization, with similar diameters as the values observed for non-functionalized particles. This means that the addition of amino groups does not lead to a size increase, however, it provokes a reduction in the agglomeration of the particles.

#### Magnetization

Magnetic properties of the particles were studied, obtaining the magnetization curves ( $M(H)$ ) of the different samples at 27°C, as shown in Figure 6. According to these  $M(H)$  curves, all the samples of nanoparticles exhibit a superparamagnetic behavior, with no hysteresis and neither coercivity nor remanence. These results are supported by previous literature, where magnetite particles show a blocking temperature (TB) of -173°C, meaning that above such temperature particles are superparamagnetic whereas below it, they are ferromagnetic [30]. Additionally, the BTD sample shows the highest value of magnetic saturation ( $M_s$ ),  $66\text{emu}\cdot\text{g}^{-1}$ , while the BC sample presents the lowest value,  $35\text{emu}\cdot\text{g}^{-1}$ . The reduction of  $M_s$  is directly related with the differences in particle size obtained by the tested synthesis methods. Batch thermal decomposition procedure needs longer reactions times than batch coprecipitation, resulting in bigger particle sizes, as was explained in the “Particles size, shape and agglomeration” discussion. Therefore, magnetic properties are considerably improved for BTD particles [45–48]. Besides, in the continuous coprecipitation, the use of a microdevice improves the control of the flowrates and residence times, which gives place to narrower size distributions. This way, a magnetic saturation value of  $49\text{emu}\cdot\text{g}^{-1}$  was achieved for the CC sample, improving the batch coprecipitation results. Moreover, the magnetic saturation for the samples BTD-BF and CC-CF are  $63\text{emu}\cdot\text{g}^{-1}$  and  $43\text{emu}\cdot\text{g}^{-1}$  respectively, so it can be assumed that particles keep their superparamagnetic behavior after being functionalized.

In view of the characterization results, it can be concluded that thermal decomposition produces particles with controlled sizes, narrow particle size distribution and improved magnetic properties. However, it is an expensive, energy-consuming, and complex method due to the large number of precursors, large volumes of reagents and high temperatures required, thus developing a more reliable and simplified technique is challenging. On the other hand, coprecipitation is a well-characterized, simple, cheap and efficient method to synthesize MNPs. Nevertheless, its bottleneck is the high tendency of the particles to agglomerate and the difficult control of their magnetic properties [49–51]. By implementing the use of microfluidics in the coprecipitation procedure, a continuous synthesis of MNPs has been achieved with reduced energy costs, small size, low reactant volume consumption and easier scale up. Furthermore, compared to batch coprecipitation, within the continuous procedure a controlled size has been obtained and therefore the surface area available for the capture reactions, the agglomeration of MNPs has been reduced and the magnetic properties of the particles have been improved.

#### Functionalization degree

The thermogravimetric analysis was performed for the different functionalized samples and the results are shown in Figure 7. In the case of non-functionalized MNPs, the samples BTD and CC, weight losses take place in the 0-250°C range of temperatures. This is associated with evaporation of traces of ethanol used in the cleaning step and in the case of BTD-BF, to the TEG that forms the particles coating [37,48]. In the case of functionalized MNPs, the weight losses in the interval 250-1000°C correspond to the losses of the anchored amino groups [40]. These functional groups losses are  $18.1\pm 1.6$ ,  $12.4\pm 6.4$  and  $8.2\pm 0.1\%$  for the samples BTD-BF,

CC-BF and CC-CF respectively. These values highlight the higher reproducibility of the functionalization process when it is developed in continuous mode. It is attributed to the use of the microdevice, where variables such as residence time and reactant flow rates can be easily adjusted, enabling higher control of the process than in batch mode.

The MNPs mass losses due to functionalization, together with the MNPs area, volume, magnetite density and weight of functional groups, have been used to estimate the grafting density of the particles, by means of Equation 2 [32–34]. This way, the number of moles of the functional group per area of particle was estimated, which can be turned into units of mass by means of Equation 3. To do so, the BET area was measured for the samples BTB-BF and CC-BF. As shown in Table 2, particles functionalized by thermal decomposition show a smaller specific area than those synthesized by coprecipitation, which can be attributed to the TEG coating of BTB-BF particles that covers the magnetite core. In the case of CC-BF, the functional groups are linked directly to the magnetite core, without any intermediate coating, which gives place to a higher specific area [37,52,53]. BET area for CC-CF was assumed equal to the one obtained for CC-BF. Finally, functionalization degree values in the order of  $10^{-4} \text{ mol}_{\text{NH}_2} \cdot \text{g}^{-1}_{\text{MNPs}}$  were obtained for the four different MNPs samples, as it can be seen in Table 2. Even though not many comparable data are available in literature, these results are of the same order of those reported by Kumar et al [54], who synthesized amino-MNPs with  $3.5 \cdot 10^{-4} \text{ mol}_{\text{NH}_2} \cdot \text{g}^{-1}_{\text{MNPs}}$  functionalization. The implementation of the functionalization step in a microfluidic device allows better control of the reactant flow rates and reduction of the reaction times. This way, a uniform layer of the functionalizing material is formed on the surface of the MNPs, obtaining functionalization degrees in the same order than within batch processes but with higher reproducibility. In addition, it implies a reduction in the reactant volume and energy consumption, resulting in less expensive, safer and more efficient systems. Finally, another advantage of the synthesis in microfluidic devices is the possibility to combine the synthesis and functionalization stages, allowing a single continuous procedure.

### 3.2 Cr(VI) capture experiments

Once the MNPs were characterized, their viability to capture Cr(VI) was tested both in batch mode and using a microfluidic device. Batch results were used as benchmark, whereas microfluidic results contributed to the development of continuous processes for the capture of pollutants in aqueous solutions. Figure 8 shows the chromium capture percentages obtained when contacting a  $23 \text{ mg} \cdot \text{L}^{-1}$  Cr(VI) solution with different BTB-BD particles suspensions. In both cases, batch (18min contact time) and continuous (18min of residence time), a decrease in the concentration of the MNPs suspension leads to a lower uptake of the target compound as expected. In continuous experiments, the capture percentage was reduced from  $93 \pm 0.1\%$  to  $56 \pm 1\%$  when MNPs concentration decreased from  $72$  to  $2.5 \text{ g}_{\text{MNPs}} \cdot \text{L}^{-1}$ . Nevertheless, no significant change in the capture percentage was observed after 18min of residence time for values  $\geq 13 \text{ g}_{\text{MNPs}} \cdot \text{L}^{-1}$ . Moreover, similar results were obtained in the experiments conducted in batch and continuous mode of operation, thus assessing the successful implementation of the microdevice in the continuous process. The small values of standard deviation proved the reproducibility of both processes. The Cr(VI) capture efficiency demonstrated by MNPs is possible thanks to their reduced size that provides a high number of active sites on their surface and to their positive charge derived from the functionalization. In addition, the high surface area of the MNPs available for the S/L contact is expected to improve the rate of the ion exchange reaction. Afterwards, it was evaluated the viability of the amino-functionalized particles for their application to polluted waters with lower concentration of chromium. To this end, an

initial Cr(VI) solution of  $500\mu\text{g}\cdot\text{L}^{-1}$  was contacted with a MNPs suspension of  $0.28\text{gMNPs}\cdot\text{L}^{-1}$ , obtaining a capture of Cr(VI) of  $82\pm 2\%$ , as shown in Figure 9. This experiment is comparable to the one in which a suspension of  $13\text{gMNPs}\cdot\text{L}^{-1}$  of BTD-BF particles is contacted with a solution with  $23\text{mg}\cdot\text{L}^{-1}$  Cr(VI) of initial concentration, achieving a Cr(VI) capture of  $86\pm 2\%$  Cr(VI). In both cases, the ratio between the initial Cr(VI) and MNPs concentration was maintained, and a contact time of 18min was applied. The similarity between the obtained capture percentages confirms the viability of the application of the functionalized MNPs particles to polluted waters with very low Cr(VI) concentrations.

Assuming ideal behavior of the contacting phases, the equilibrium constant for the ion exchange reaction (Equation 5) can be defined as shown in Equation 8.  $[\text{HCrO}_4^-]$  refers to the equilibrium Cr concentration in solution, measured by ICP;  $[\text{NH}_n^+ \cdot \text{HCrO}_4^-]$  corresponds to the equilibrium concentration of Cr(VI) captured by the MNPs, calculated after applying the mass balance between the known initial Cr(VI) concentration in solution and the measured equilibrium Cr(VI) concentration in solution;  $[\text{Cl}^-]$  is the equilibrium chloride concentration in solution, which is considered equal to  $[\text{NH}_n^+ \cdot \text{HCrO}_4^-]$ , assuming the stoichiometric ratio 1:1;  $[\text{NH}_n^+ \cdot \text{Cl}^-]$  is the concentration of chloride groups on the nanoparticles at equilibrium. Assuming that initially every amino functional group is linked to a chloride ion, this value is calculated after the mass balance to the known functional group concentration in the surface of MNPs and the calculated equilibrium chloride concentration in solution. The functional group concentration in the surface of MNPs can be obtained by means of the functionalization degree estimated in section 3.1 “MNPs characterization”.

$$K_{eq} = \frac{[\text{NH}_n^+ \cdot \text{HCrO}_4^-][\text{Cl}^-]}{[\text{NH}_n^+ \cdot \text{Cl}^-][\text{HCrO}_4^-]} \quad (8)$$

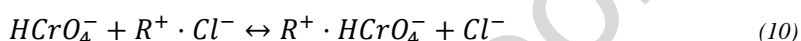
This expression can be rearranged and linearized to yield Equation 9:

$$\frac{1}{D_1} = K_{eq} \cdot \frac{1}{D_2} \quad (9)$$

where D1 and D2 represent respectively the ratio of chromate and chloride anchored to the MNPs to the concentration of the ion remaining in the aqueous phase [14]. To obtain the value of the equilibrium constant, fitting of the experimental data to Equation 9 was performed. Therefore, a value of  $K_{eq}=1.51[-]$ , with  $R^2=0.98$ , was obtained. Additionally, the Cr(VI) exchange capacity of the particles was calculated for the different experimental conditions applying Equation 7, this way a maximum exchange capacity of  $5.2\text{mg}_{\text{Cr(VI)}}\cdot\text{g}^{-1}_{\text{MNPs}}$  was obtained for BTD-BF particles in the studied MNPs concentration interval. Experiments were also performed with continuously synthesized CC-CF particles, with a residence time of 18min. As shown in Figure 9, when a  $23\text{mg}\cdot\text{L}^{-1}$  solution was contacted with a suspension of  $13\text{g}_{\text{MNPs}}\cdot\text{L}^{-1}$ , a complete capture of hexavalent chromium ( $97\pm 2\%$ ) was achieved, the same that happened with BTD-BF particles. Moreover, a  $54\pm 3\%$  of the initial Cr(VI) was captured with a  $1\text{g}_{\text{MNPs}}\cdot\text{L}^{-1}$  CC-CF suspension. Applying Equation 7, a maximum exchange capacity of  $12.5\text{mg}_{\text{Cr(VI)}}\cdot\text{g}^{-1}_{\text{MNPs}}$  was obtained for these particles in the studied MNPs concentration interval. The difference between BTD-BF and CC-CF maximum capacities is due to the lower size and higher functionalization degree presented by particles synthesized with continuous coprecipitation and continuous functionalization. The maximum exchange capacities of both samples of particles have been expressed in terms of  $\text{meq}_{\text{Cr(VI)}}\cdot\text{g}^{-1}_{\text{MNPs}}$  for comparison with the exchange capacity values of commercial ion exchange resins, as shown in Table 3.

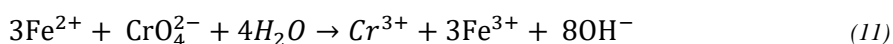
Ion exchange processes have been widely applied for the separation of heavy metals from wastewaters, working both with ion exchange extractants in liquid-liquid contact and with ion exchange resins in solid-liquid contact. High capture efficiencies and kinetics have been

reported working with tertiary amines [14,15,55] and quaternary ammonium salts [7–10,56,57]. Ion exchange resins follow the same principles and characteristics regarding the ion exchange reaction but report the advantage of working with an easily manageable solid phase. Several commercial macroporous-type anion exchange resins, formed by micrometric particles, have been studied in literature for the removal of Cr(VI) from aqueous solutions, for example Lewatit MP 62, a weakly basic resin made of crosslinked polystyrene; Lewatit M610, a strongly basic with a crosslinked polystyrene matrix [55]; Lewatit MP 64, a weakly basic and Lewatit MP 500, a strongly basic resin, both made of Styrene-polystyrene [12,57]. In all these works, the resins have been conditioned with HCl previous to the contact with the Cr(VI) solution, thus the capture reaction took place at acidic pH (below 6), in which  $\text{HCrO}_4^-$  is the most predominant Cr(VI) specie and the ion exchange stoichiometric reaction follows Equation 10, being R the resin functional group. In the case of the MNPs technology, the R term refers to the functionalization of the particles, which is based on primary and secondary amino groups (Equation 5).



In this work and for the sake of clarity, a simple comparison in terms of maximum Cr(VI) capture capacity between the synthesized MNPs and some commercial resins is provided. Table 3 summarizes the initial conditions and equilibrium parameters. The different results of the equilibrium constants in the ion exchange resin studies, remark the high influence of the type of resin and operational conditions in the Cr(VI) capture. The maximum exchange capacity showed by continuously synthesized MNPs is in the range of previously reported commercial ion exchange resins data, having as an additional advantage the considerable smaller size of MNPs (BTD-BF: 12.3nm; CC-CF: 8.8nm) than the ion exchange beads (590 $\mu\text{m}$ ), which leads to a higher surface area for the S/L contact, parameter that would greatly affect and improve the capture rate, increasing the potential for continuous processes. MNPs also present chemical stability, good dispersibility in water, low intraparticle diffusion rate and thus, they exhibit fast kinetics, good selectivity, and allow for the intensification of the process. In addition, although not included in the present work, the superparamagnetic character of the solid phase allows for their continuous separation from the liquid medium as part of a continuous capture and separation process, which can take place in one single taylor made microdevice or in a microdevices array [4,27,29].

Besides, experiments with CC continuously synthesized particles have been developed to compare the activity of amino-functionalized MNPs and bare magnetite MNPs. After a contact time of 18min and with an initial Cr(VI) concentration of 23mg $\cdot\text{L}^{-1}$ , the percentage of Cr(VI) uptake with a suspension of 13g $_{\text{MNPs}}\cdot\text{L}^{-1}$  CC was 2.5 $\pm$ 0.1% . As shown in Figure 9, this value is considerably lower than the results obtained when using functionalized particles. When contacting with a 1g $_{\text{MNPs}}\cdot\text{L}^{-1}$ , the Cr(VI) capture percentage is reduced to 0.7 $\pm$ 0.1%. Applying Equation 7, a maximum Cr(VI) capture capacity of 0.02meq $_{\text{Cr(VI)}}\cdot\text{g}^{-1}_{\text{MNPs}}$  was obtained for bare magnetite particles in the studied MNPs concentration interval. It is two orders of magnitude lower than the value previously obtained for the amino-functionalized MNPs continuously synthesized in this work, applying the same experimental conditions. This remarks the importance of the functionalization step, to convert the magnetic cores into robust MNPs with high performance in the retention of Cr(VI) anions; this behavior could be extended to other anionic pollutants. The mechanism of removal of Cr(VI) by bare magnetite particles consists on reducing Cr(VI) ions to Cr(III) by the irreversible REDOX reaction shown in Equation 11 [58–62].



However, this irreversible reaction limits the regeneration of the loaded particles, giving place to poor efficiencies in their reuse. This is supported by results obtained in literature, for example, reutility efficiencies of 35.6% were reported by Yuan, P. et al [58] for the first regeneration-reuse cycle, of 14.3% for the second cycle and only of 6.3% for the third. These low values convert magnetite nanoparticles into single-use adsorbents, being disadvantageous from the economic and environmental aspects. In this work, the mechanism for Cr(VI) removal consist in its capture by amino-functionalized particles, based on the reversible ion exchange reaction presented in Equation 5. The advantage of working with this system is that loaded MNPs can be easily regenerated and successfully recycled many times, similar to the process with different ion exchange resins.

The viability of the amino-functionalized MNPs for their regeneration and reuse has been tested in this work with a BTD-BD MNPs suspension of  $2.5\text{g}_{\text{MNPs}}\cdot\text{L}^{-1}$ , using a second spiral shape microdevice connected to the capture stage, and results are shown in Figure 10. After their protonation with HCl (Equation 1), the 0.44 mM MNPs solution presents a pH of 4, and thus, a high and positive zeta potential, as was analyzed in Section 3.1 “MNPs characterization”. Under this conditions, they are able to capture a  $56\pm 1\%$  of the initial Cr(VI), as seen in Section 3.2 “Cr(VI) capture experiments”. Afterwards, a 0.02M NaOH solution was added in the second microreactor and its contact with the Cr(VI) loaded MNPs took place with a residence time of 9min. This NaOH addition gave place to a change of the pH of the solution to a basic form (pH12), resulting in negative values of the particle’s zeta potential. These negative surface charge indicates that particles are in anionic form, as they have been deprotonated due to the NaOH addition, and thus, a  $94 \pm 6\%$  of the Cr(VI) has been released to the liquid phase, only remaining a  $6 \pm 6\%$  of the initial Cr(VI) in the particles surface. These results remark that both the capture and regeneration stages are favoured by the small nanometric size of MNPs that greatly improves the capture rate. This way, with adequate residence times (capture: 18min; regeneration: 9min) the equilibrium is achieved in both stages. Afterwards, particles were protonated again with a 0.01M HCl solution and reused for the capture stage, achieving a  $57 \pm 14\%$  of Cr(VI) intake, very similar to the percentage obtained in the first Cr(VI) capture cycle. It means that once the particles are regenerated the capture efficiency is kept constant. All these characteristics make MNPs a stable, efficient, and cost-effective materials to be employed for the capture of Cr(VI) from aqueous solutions as well as for the capture of different pollutants from complex fluids after the adequate functionalization.

#### 4. CONCLUSIONS AND FUTURE WORK

This study contributes to the design of robust microfluidic systems for the continuous, rapid and effective capture of aqueous pollutants using functionalized magnetic nanoparticles; more specifically, the capture of Cr(VI) present in aqueous solutions with amino-MNPs has been selected as representative case of study. In this environmental application, selectivity and capture rate are paramount and usually face a tedious process in the synthesis and functionalization of the particles. Therefore, in this work, the most recent strategy for the synthesis of MNPs has been applied, consisting of the implementation of microfluidics for the continuous and highly controlled production of functionalized MNPs. Compared to batch results, controlled sizes were obtained, higher reproducibilities were achieved, agglomeration was considerably reduced, magnetic properties were enhanced, and reactant and energy consumptions were lowered. Afterwards, the continuous Cr(VI) capture was studied by changing the concentration of the MNPs suspension. Continuously synthesized and functionalized MNPs (CC-CF) showed a maximum retention capacity of  $1.44\text{ meq}_{\text{Cr(VI)}}\cdot\text{g}^{-1}_{\text{MNPs}}$ ,

higher than obtained values for bare magnetite MNPs (CC) and batch synthesized and functionalized MNPs (BTD-BF), due to their lower size and higher amino-functionalization. This value is also in the range of previously reported commercial ion exchange resins values, besides, it is worth highlighting the considerable smaller size of MNPs than the ion exchange beads, that leads to a higher surface area in the S/L contact, improving the capture rate due to the higher surface area available and lower influence of internal diffusion phenomena. The latter, again showed advantage in the regeneration rate of the loaded MNPs. Additionally, the superparamagnetic character of the MNPs allows for their continuous separation from the liquid medium after the capture stage studied in this work, and as a part of the continuous separation process. Moreover, the regeneration of the loaded MNPs has been proved changing their superficial charge, then particles were recycled demonstrating that capture efficiency was kept constant. All these characteristics make amino-functionalized MNPs a promising, energy efficient and cost-effective alternative for the capture of charged molecules from aqueous solutions using microdevices.

The successful implementation of microfluidics in the different stages of the process: synthesis of MNPs, functionalization with amino groups, selective capture of Cr(VI) from aqueous solutions and regeneration of loaded MNPs, remarks the possibility to take advantage of the use of microdevices. Their application allows to reduce energy costs and reactant volume consumption, to promote better control on the process variables than in batch, such as microchannel diameter or reactant flow rates, to improve mass and heat transfer and to flow within the laminar regime with small residence times. Collectively, the system and methodology here reported can be of high use in assessing the performance of new materials, including their synthesis, for the selective capture of aqueous pollutants as a preliminary step to process design and scale-up. Furthermore, it has been confirmed the possible extension of the reported methodology to polluted waters with very low Cr(VI) concentrations, in the order of  $\mu\text{g}\cdot\text{L}^{-1}$ .

## 5. Acknowledgements

Financial support from the Spanish Ministry of Science and Innovation under project RTI2018-093310-B-I00 (MCI/AEI/FEDER, UE) is gratefully acknowledged. Belén García-Merino also thank the FPI research grant PRE2019-089339.

## 6. References

- [1] L. Wu, A. Mendoza-Garcia, Q. Li, S. Sun, Organic Phase Syntheses of Magnetic Nanoparticles and Their Applications, *Chemical Reviews*. 116 (2016) 10473–10512. <https://doi.org/10.1021/acs.chemrev.5b00687>.
- [2] J. Gómez-Pastora, Application and separation of magnetic micro- and nanomaterials, in: Universidad de Cantabria (Ed.), *On the Design of Lab-on-a-Chip Devices for Magnetophoretic Separations*, PhD thesis, Santander, España, 2018.
- [3] Z. Chen, C. Wu, Z. Zhang, W. Wu, X. Wang, Z. Yu, Synthesis, functionalization, and nanomedical applications of functional magnetic nanoparticles, *Chinese Chemical Letters*. 29 (2018) 1601–1608. <https://doi.org/10.1016/j.ccllet.2018.08.007>.
- [4] F. Gao, An Overview of Surface-Functionalized Magnetic Nanoparticles: Preparation and Application for Wastewater Treatment, *Chemistry Select*. 4 (2019) 6805–6811. <https://doi.org/10.1002/slct.201900701>.

- [5] J.H. Jung, J.H. Lee, S. Shinkai, Functionalized magnetic nanoparticles as chemosensors and adsorbents for toxic metal ions in environmental and biological fields, *Chemical Society Reviews*. 40 (2011) 4464–4474. <https://doi.org/10.1039/c1cs15051k>.
- [6] R.A. Bohara, N.D. Thorat, S.H. Pawar, Role of functionalization: Strategies to explore potential nano-bio applications of magnetic nanoparticles, *RSC Advances*. 6 (2016) 43989–44012. <https://doi.org/10.1039/c6ra02129h>.
- [7] E. Salazar, M.I. Ortiz, A.M. Urtiaga, J.A. Irabien, Equilibrium and Kinetics of Cr(VI) Extraction with Aliquat 336, *Industrial and Engineering Chemistry Research*. 31 (1992) 1516–1522. <https://doi.org/10.1021/ie00006a014>.
- [8] B. Galán, A.M. Urtiaga, A.I. Alonso, J.A. Irabien, M.I. Ortiz, Extraction of Anions with Aliquat 336: Chemical Equilibrium Modeling, *Industrial and Engineering Chemistry Research*. 33 (1994) 1765–1770. <https://doi.org/10.1021/ie00031a015>.
- [9] A.I. Alonso, A.M. Urtiaga, A. Irabien, M. Inmaculada Ortiz, Extraction of Cr(VI) with aliquat 336 in hollow fiber contactors: mass transfer analysis and modeling, *Chemical Engineering Science*. 49 (1994) 901–909. [https://doi.org/10.1016/0009-2509\(94\)80026-X](https://doi.org/10.1016/0009-2509(94)80026-X).
- [10] A.I. Alonso, B. Galán, A. Irabien, I. Ortiz, Separation of Cr(VI) with Allquat 336: Chemical Equilibrium Modeling, *Separation Science and Technology*. 32 (1997) 1543–1555. <https://doi.org/10.1080/01496399708004065>.
- [11] W.S.W. Ho, T.K. Poddar, New Membrane Technology for Removal and Recovery of Chromium from Waste Waters, *Environmental Progress*. 20 (2001) 44–52. <https://doi.org/https://doi.org/10.1002/ep.670200115>.
- [12] M.J. Rivero, O. Primo, M.I. Ortiz, Modelling of Cr(VI) removal from polluted groundwaters by ion exchange, *Journal of Chemical Technology and Biotechnology*. 79 (2004) 822–829. <https://doi.org/10.1002/jctb.1049>.
- [13] B. Galán, D. Castañeda, I. Ortiz, Removal and recovery of Cr(VI) from polluted ground waters: A comparative study of ion-exchange technologies, *Water Research*. 39 (2005) 4317–4324. <https://doi.org/https://doi.org/10.1016/j.watres.2005.08.015>.
- [14] E. Bringas, M.F. San Román, I. Ortiz, Removal of anionic pollutants from groundwaters using Alamine 336: chemical equilibrium modelling, *Journal of Chemical Technology & Biotechnology*. 81 (2006) 1829–1835. <https://doi.org/10.1002/jctb>.
- [15] A. Basauri, J. Gómez-Pastora, M. Fallanza, E. Bringas, I. Ortiz, Predictive model for the design of reactive micro-separations, *Separation and Purification Technology*. 209 (2019) 900–907. <https://doi.org/10.1016/j.seppur.2018.09.028>.
- [16] X. Zhao, X. Yu, X. Wang, S. Lai, Y. Sun, D. Yang, Recent advances in metal-organic frameworks for the removal of heavy metal oxoanions from water, *Chemical Engineering Journal*. 407 (2021) 127221. <https://doi.org/10.1016/j.cej.2020.127221>.
- [17] R. Zhang, D. Li, J. Sun, Y. Cui, Y. Sun, In situ synthesis of FeS/Carbon fibers for the effective removal of Cr(VI) in aqueous solution, *Frontiers of Environmental Science and Engineering*. 14 (2020) 68. <https://doi.org/10.1007/s11783-020-1247-8>.

- [18] S.A. Elfeky, S.E. Mahmoud, A.F. Youssef, Applications of CTAB modified magnetic nanoparticles for removal of chromium (VI) from contaminated water, *Journal of Advanced Research*. 8 (2017) 435–443. <https://doi.org/10.1016/j.jare.2017.06.002>.
- [19] R. Wang, K. Chen, S. Peng, Q.Y. Wang, S.H. Huang, Q.H. Zhou, J. Wang, J. Lin, Environmentally friendly magnetic nanoparticles for efficient removal of methylene blue and cr(vi) from water, *Nano*. 15 (2020) 1–14. <https://doi.org/10.1142/S1793292020050126X>.
- [20] K. Chithra, R.T. Akshayaraj, K. Pandian, Polypyrrole-Protected Magnetic Nanoparticles as an Excellent Sorbent for Effective Removal of Cr(VI) and Ni(II) from Effluent Water: Kinetic Studies and Error Analysis, *Arabian Journal for Science and Engineering*. 43 (2018) 6219–6228. <https://doi.org/10.1007/s13369-018-3421-x>.
- [21] A. Debnath, M. Majumder, M. Pal, N.S. Das, K.K. Chattopadhyay, B. Saha, Enhanced Adsorption of Hexavalent Chromium onto Magnetic Calcium Ferrite Nanoparticles: Kinetic, Isotherm, and Neural Network Modeling, *Journal of Dispersion Science and Technology*. 37 (2016) 1806–1818. <https://doi.org/10.1080/01932691.2016.1141100>.
- [22] J. Gómez-Pastora, C. González-Fernández, E. Real, A. Iles, E. Bringas, E.P. Furlani, I. Ortiz, Computational modeling and fluorescence microscopy characterization of a two-phase magnetophoretic microsystem for continuous-flow blood detoxification, *Lab on a Chip*. 18 (2018) 1593–1606. <https://doi.org/10.1039/c8lc00396c>.
- [23] C. González Fernández, J. Gómez-Pastora, A. Basauri, M. Fallanza, E. Bringas, J.J. Chalmers, I. Ortiz, Continuous-Flow Separation of Magnetic Particles from Biofluids: How Does the Microdevice Geometry Determine the Separation Performance?, *Sensors*. 20 (2020) 3030. <https://doi.org/10.3390/s20113030>.
- [24] Y. Zhou, Y. wang, Q. Lin, A Microfluidic Device for Continuous-Flow Magnetically Controlled Capture and Isolation of Microparticles, *J Microelectromech Syst*. 19 (2010) 743–751. <https://doi.org/10.1109/JMEMS.2010.2050194.A>.
- [25] J. Mosayebi, M. Kiyasatfar, S. Laurent, Synthesis, functionalization, and design of magnetic nanoparticles for theranostic applications, 2017. <https://doi.org/10.1002/adhm.201700306>.
- [26] S.A.M.K. Ansari, E. Ficiarà, F.A. Ruffinatti, I. Stura, M. Argenziano, O. Abollino, R. Cavalli, C. Guiot, F. D'Agata, Magnetic iron oxide nanoparticles: Synthesis, characterization and functionalization for biomedical applications in the Central Nervous System, *Materials*. 12 (2019) 465. <https://doi.org/10.3390/ma12030465>.
- [27] B. García-Merino, E. Bringas, I. Ortiz, Synthesis and applications of surface-modified magnetic nanoparticles: Progress and future prospects, *Reviews in Chemical Engineering*. (2021) 000010151520200072. <https://doi.org/10.1515/revce-2020-0072>.
- [28] J. Saiz, E. Bringas, I. Ortiz, Functionalized magnetic nanoparticles as new adsorption materials for arsenic removal from polluted waters, *Journal of Chemical Technology and Biotechnology*. 89 (2014) 909–918. <https://doi.org/10.1002/jctb.4331>.
- [29] J. Gómez-Pastora, E. Bringas, I. Ortiz, Recent progress and future challenges on the use of high performance magnetic nano-adsorbents in environmental applications,

- Chemical Engineering Journal. 256 (2014) 187–204.  
<https://doi.org/10.1016/j.cej.2014.06.119>.
- [30] W. Cai, J. Wan, Facile synthesis of superparamagnetic magnetite nanoparticles in liquid polyols, *Journal of Colloid and Interface Science*. 305 (2007) 366–370.  
<https://doi.org/10.1016/j.jcis.2006.10.023>.
- [31] M.O. Besenhard, A.P. LaGrow, A. Hodzic, M. Kriechbaum, L. Panariello, G. Bais, K. Loizou, S. Damilos, M. Margarida Cruz, N.T.K. Thanh, A. Gavriilidis, Co-precipitation synthesis of stable iron oxide nanoparticles with NaOH: New insights and continuous production via flow chemistry, *Chemical Engineering Journal*. 399 (2020) 125740.  
<https://doi.org/10.1016/j.cej.2020.125740>.
- [32] L. Zeininger, S. Petzi, J. Schönamsgruber, L. Portilla, M. Halik, A. Hirsch, Very Facile Polarity Umpolung and Noncovalent Functionalization of Inorganic Nanoparticles: A Tool Kit for Supramolecular Materials Chemistry, *Chemistry - A European Journal*. 21 (2015) 14030–14035. <https://doi.org/10.1002/chem.201501682>.
- [33] D.N. Benoit, H. Zhu, M.H. Lillierose, R.A. Verm, N. Ali, A.N. Morrison, J.D. Fortner, C. Avendano, V.L. Colvin, Measuring the grafting density of nanoparticles in solution by analytical ultracentrifugation and total organic carbon analysis, *Analytical Chemistry*. 84 (2012) 9238–9245. <https://doi.org/10.1021/ac301980a>.
- [34] G. Leone, U. Giovanella, F. Bertini, W. Porzio, F. Meinardi, C. Botta, G. Ricci, Poly(styrene)-graft-/rhodamine 6G- fluoromica hybrids: synthesis, characterization and photophysical properties, *J. Mater. Chem. C*. 7 (2013) 10715–10722.  
<https://doi.org/10.1039/b000000x>.
- [35] P.J. Harrington, G.W. Stevens, Study of Cr(VI)/Tertiary amine reaction kinetics using a modified rotating diffusion cell, *Solvent Extraction and Ion Exchange*. 18 (2000) 907–932. <https://doi.org/10.1080/07366290008934714>.
- [36] D. Maity, P. Chandrasekharan, C.T. Yang, K.H. Chuang, B. Shuter, J.M. Xue, J. Ding, S.S. Feng, Facile synthesis of water-stable magnetite nanoparticles for clinical MRI and magnetic hyperthermia applications, *Nanomedicine*. 5 (2010) 1571–1584.  
<https://doi.org/10.2217/nnm.10.77>.
- [37] J.K. Sahoo, S.K. Paikra, M. Mishra, H. Sahoo, Amine functionalized magnetic iron oxide nanoparticles: Synthesis, antibacterial activity and rapid removal of Congo red dye, *Journal of Molecular Liquids*. 282 (2019) 428–440.  
<https://doi.org/10.1016/j.molliq.2019.03.033>.
- [38] Z. Mokadem, S. Mekki, S. Saïdi-Besbes, G. Agusti, A. Elaissari, A. Derdour, Triazole containing magnetic core-silica shell nanoparticles for Pb<sup>2+</sup>, Cu<sup>2+</sup> and Zn<sup>2+</sup> removal, *Arabian Journal of Chemistry*. 10 (2017) 1039–1051.  
<https://doi.org/10.1016/j.arabjc.2016.12.008>.
- [39] R.A. Bini, R.F.C. Marques, F.J. Santos, J.A. Chaker, M. Jafelicci, Synthesis and functionalization of magnetite nanoparticles with different amino-functional alkoxysilanes, *Journal of Magnetism and Magnetic Materials*. 324 (2012) 534–539.  
<https://doi.org/10.1016/j.jmmm.2011.08.035>.

- [40] J. Saiz, Síntesis y caracterización de nanomateriales funcionalizados, in: Universidad de Cantabria (Ed.), *Diseño de Nanoadsorbentes Magnéticos Funcionalizados Para La Eliminación de Arsénico de Aguas Subterráneas Contaminadas*, PhD thesis, Santander, España, 2015: pp. 41–84.
- [41] M.J. Kim, Y.H. Choa, D.H. Kim, K.H. Kim, Magnetic behaviors of surface modified superparamagnetic magnetite nanoparticles, *IEEE Transactions on Magnetics*. 45 (2009) 2446–2449. <https://doi.org/10.1109/TMAG.2009.2018606>.
- [42] K. Hayashi, H. Tomonaga, T. Matsuyama, J. Ida, Facile synthesis, characterization of various polymer immobilized on magnetite nanoparticles applying the coprecipitation method, *Journal of Applied Polymer Science*. 139 (2021) 51581. <https://doi.org/10.1002/app.51581>.
- [43] A.Z.M. Badruddoza, Z.B.Z. Shawon, M.T. Rahman, K.W. Hao, K. Hidajat, M.S. Uddin, Ionically modified magnetic nanomaterials for arsenic and chromium removal from water, *Chemical Engineering Journal*. 225 (2013) 607–615. <https://doi.org/10.1016/j.cej.2013.03.114>.
- [44] P.L. Suryawanshi, S.H. Sonawane, B.A. Bhanvase, M. Ashokkumar, M.S. Pimplapure, P.R. Gogate, Synthesis of iron oxide nanoparticles in a continuous flow spiral microreactor and Corning® advanced flow™ reactor, *Green Processing and Synthesis*. 7 (2018) 1–11. <https://doi.org/10.1515/gps-2016-0138>.
- [45] H.K. Kim, J.W. Park, Agglomeration of 10 nm amine-functionalized nano-magnetite does not hinder its efficiency as an environmental adsorbent, *Journal of Environmental Science and Health - Part A Toxic/Hazardous Substances and Environmental Engineering*. 54 (2019) 648–656. <https://doi.org/10.1080/10934529.2019.1579535>.
- [46] M.C. Mascolo, Y. Pei, T.A. Ring, Room Temperature Co-Precipitation Synthesis of Magnetite Nanoparticles in a Large pH Window with Different Bases, *Materials*. 6 (2013) 5549–5567. <https://doi.org/10.3390/ma6125549>.
- [47] S. Nejabat, S.O.R. Siadat, Z. Tahmasian, F. Mirzajani, F. Fatemi, S. Hosseinkhani, M.R. Abedi, How Co-Precipitation Reaction Parameters Control the Characteristics and Features of Iron Oxide Nanoparticles, *Physical Chemistry Research*. 9 (2021) 242–252. <https://doi.org/10.22036/pcr.2020.251463.1843>.
- [48] M. Singh, N. Sviridenkova, N. Timur, A. Savchenko, I. Shetinin, A. Majouga, Synthesis and Characterization of Stable Iron Oxide Nanoparticle with Amino Covalent Binding on the Surface for Biomedical Application, *Journal of Cluster Science*. 27 (2016) 1383–1393. <https://doi.org/10.1007/s10876-016-1007-x>.
- [49] S. Kaliamurthi, A. Demir-Korkmaz, G. Selvaraj, E. Gokce-Polat, Y.-K. Wei, M.A. Almessiere, A. Baykal, K. Gu, D.-Q. Wei, Viewing the Emphasis on State-of-the-Art Magnetic Nanoparticles: Synthesis, Physical Properties, and Applications in Cancer Theranostics, *Current Pharmaceutical Design*. 25 (2019) 1505–1523. <https://doi.org/10.2174/1381612825666190523105004>.
- [50] A. Yadollahpour, Magnetic nanoparticles in medicine: A review of synthesis methods and important characteristics, *Oriental Journal of Chemistry*. 31 (2015) 271–277. <https://doi.org/10.13005/ojc/31.Special-Issue1.33>.

- [51] K.N. Koo, A.F. Ismail, M.H.D. Othman, N. Bidin, M. A Rahman, Preparation and characterization of superparamagnetic magnetite (Fe<sub>3</sub>O<sub>4</sub>) nanoparticles: A short review, *Malaysian Journal of Fundamental and Applied Sciences*. 15 (2019) 23–31. <https://doi.org/10.11113/mjfas.v15n2019.1224>.
- [52] J. Kim, J. Gómez-Pastora, C.J. Gilbert, M. Weigand, N.A. Walters, E. Reátegui, A.F. Palmer, M. Yazer, M. Zborowski, J.J. Chalmers, Quantification of the Mean and Distribution of Hemoglobin Content in Normal Human Blood Using Cell Tracking Velocimetry, *Analytical Chemistry*. 92 (2019) 1956–1962. <https://doi.org/10.1021/acs.analchem.9b04302>.
- [53] Y. Lin, H. Chen, K. Lin, B. Chen, C. Chiou, Application of magnetic particles modified with amino groups to adsorb copper ions in aqueous solution, *Journal of Environmental Sciences*. 23 (2011) 44–50. [https://doi.org/10.1016/S1001-0742\(10\)60371-3](https://doi.org/10.1016/S1001-0742(10)60371-3).
- [54] S. Kumar, A.K. Jana, I. Dhamija, Y. Singla, M. Maiti, Preparation, characterization and targeted delivery of serratiopeptidase immobilized on amino-functionalized magnetic nanoparticles, *European Journal of Pharmaceutics and Biopharmaceutics*. 85 (2013) 413–426. <https://doi.org/10.1016/j.ejpb.2013.06.019>.
- [55] F. Gode, E. Pehlivan, Removal of Cr(VI) from aqueous solution by two Lewatit-anion exchange resins, *Journal of Hazardous Materials*. 119 (2005) 175–182. <https://doi.org/10.1016/j.jhazmat.2004.12.004>.
- [56] B. Galán, M. Calzada, I. Ortiz, Recycling of Cr(VI) by membrane solvent extraction: Long term performance with the mathematical model, *Chemical Engineering Journal*. 124 (2006) 71–79. <https://doi.org/10.1016/j.cej.2006.07.009>.
- [57] E. Pehlivan, S. Cetin, Sorption of Cr(VI) ions on two Lewatit-anion exchange resins and their quantitative determination using UV-visible spectrophotometer, *Journal of Hazardous Materials*. 163 (2009) 448–453. <https://doi.org/10.1016/j.jhazmat.2008.06.115>.
- [58] P. Yuan, D. Liu, M. Fan, D. Yang, R. Zhu, F. Ge, J.X. Zhu, H. He, Removal of hexavalent chromium [Cr(VI)] from aqueous solutions by the diatomite-supported/unsupported magnetite nanoparticles, *Journal of Hazardous Materials*. 173 (2010) 614–621. <https://doi.org/10.1016/j.jhazmat.2009.08.129>.
- [59] T.E. Abilio, B.C. Soares, J.C. José, P.A. Milani, G. Labuto, E.N.V.M. Carrilho, Hexavalent chromium removal from water: adsorption properties of in natura and magnetic nanomodified sugarcane bagasse, *Environmental Science and Pollution Research*. 28 (2021) 24816–24829. <https://doi.org/10.1007/s11356-020-11726-8>.
- [60] J. Hu, I.M.C. Lo, G. Chen, Removal of Cr(VI) by magnetite nanoparticle, *Water Science Technology*. 50 (2004) 139–146. <https://iwaponline.com/wst/article-pdf/50/12/139/47136/139.pdf>.
- [61] M.L. Peterson, G.E. Brown, G.A. Parks, Direct XAFS evidence for heterogeneous redox reaction at the aqueous chromium/magnetite interface, *Colloids and Surfaces A: Physicochemical and Engineering Aspects*. 107 (1996) 77–88. [https://doi.org/https://doi.org/10.1016/0927-7757\(95\)03345-9](https://doi.org/https://doi.org/10.1016/0927-7757(95)03345-9).

- [62] Maria L. Peterson, A.F. White, G.E. Brown, G.A. Parks, Surface Passivation of Magnetite by Reaction with Aqueous Cr(VI): XAFS and TEM Results, *Environ Sci Technol.* 31 (1997) 1573–1576. <https://doi.org/https://doi.org/10.1021/es960868i>.

Journal Pre-proof

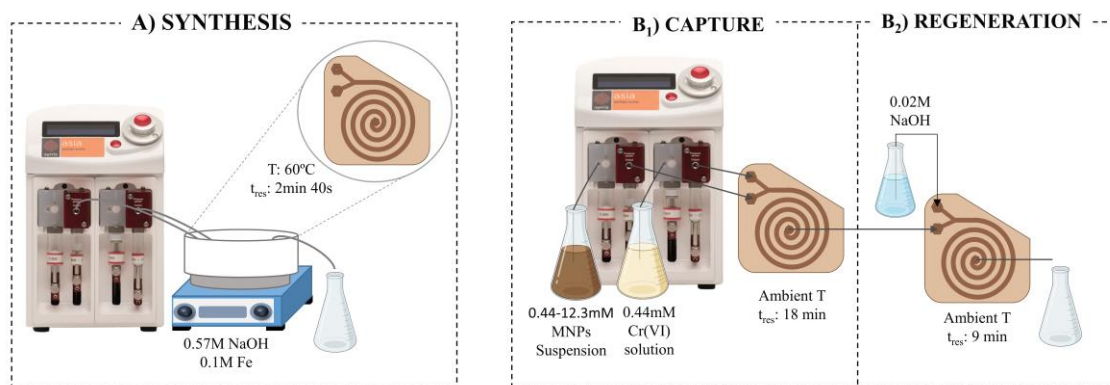


Figure 1. Experimental set up of the microfluidic process including A) continuous coprecipitation, B1) Cr (VI) continuous capture experiments and B2) Regeneration of MNPs. Microfluidic system: Spiral shape microreactor with 400mm length and a circular section of 3mm diameter, TFE tubing (0.3mm ID and 1.58 mm OD) and pressure pump (Asia Flow Chemistry Syringe Pump, Syrris).

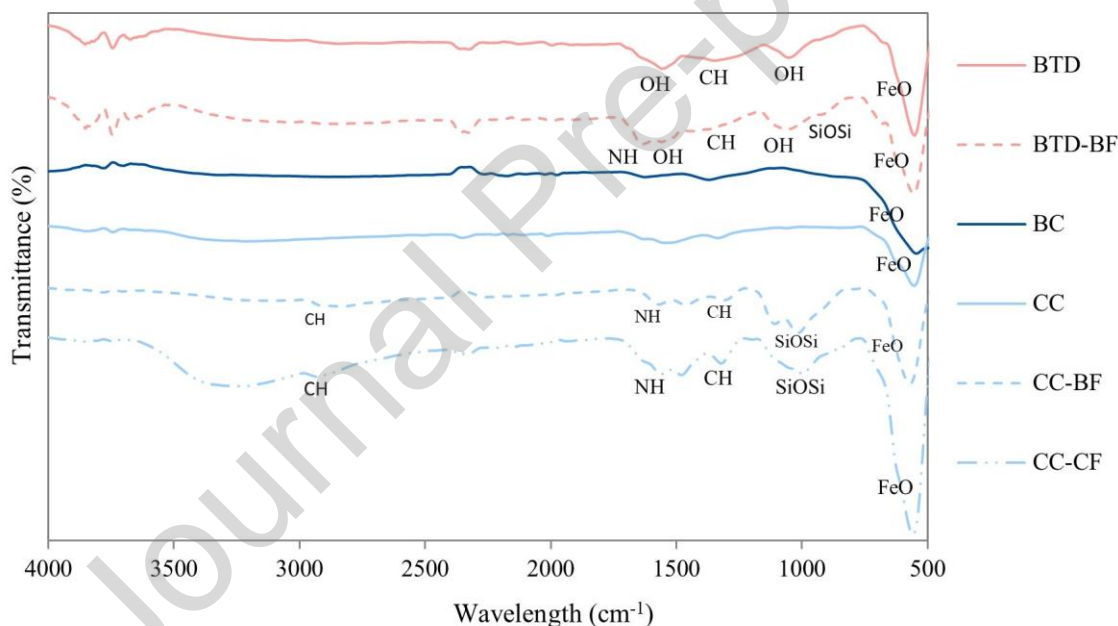


Figure 2. FTIR spectra of the different MNPs samples synthesized by batch thermal decomposition (BTD), batch thermal decomposition followed by batch amino-functionalization (BTD-BF), batch coprecipitation (BC), continuous coprecipitation (CC), continuous coprecipitation followed by batch amino-functionalization (CC-BF) and continuous coprecipitation followed by continuous amino-functionalization (CC-CF).

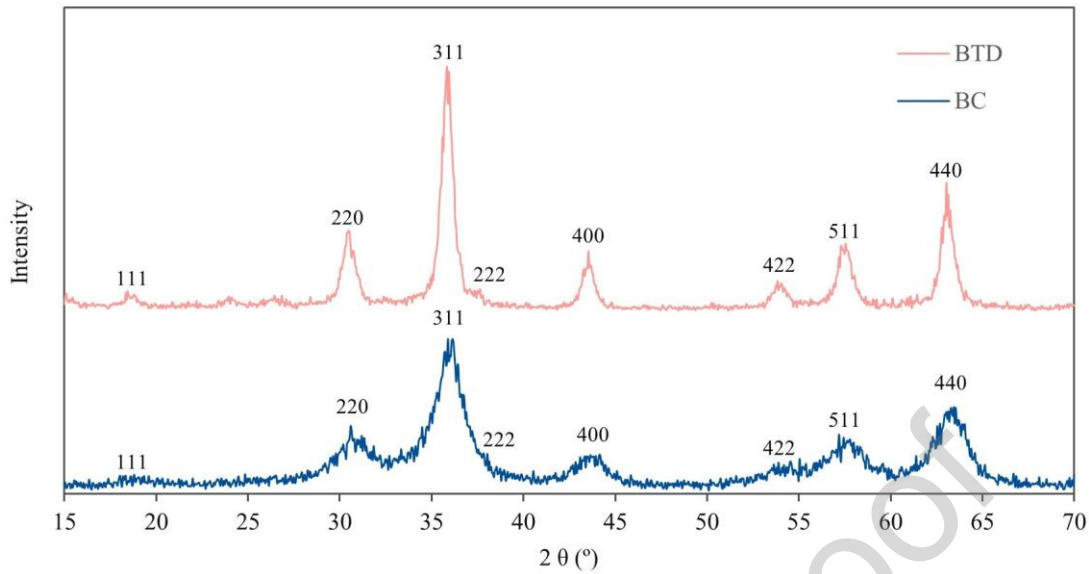


Figure 3. X-ray diffraction spectra of the MNPs samples synthesized by batch thermal decomposition (BTD) and batch coprecipitation (BC). Numbers indicate the peaks position and the Miller indexes of the reference structure: magnetite (ICDD, PDF2).

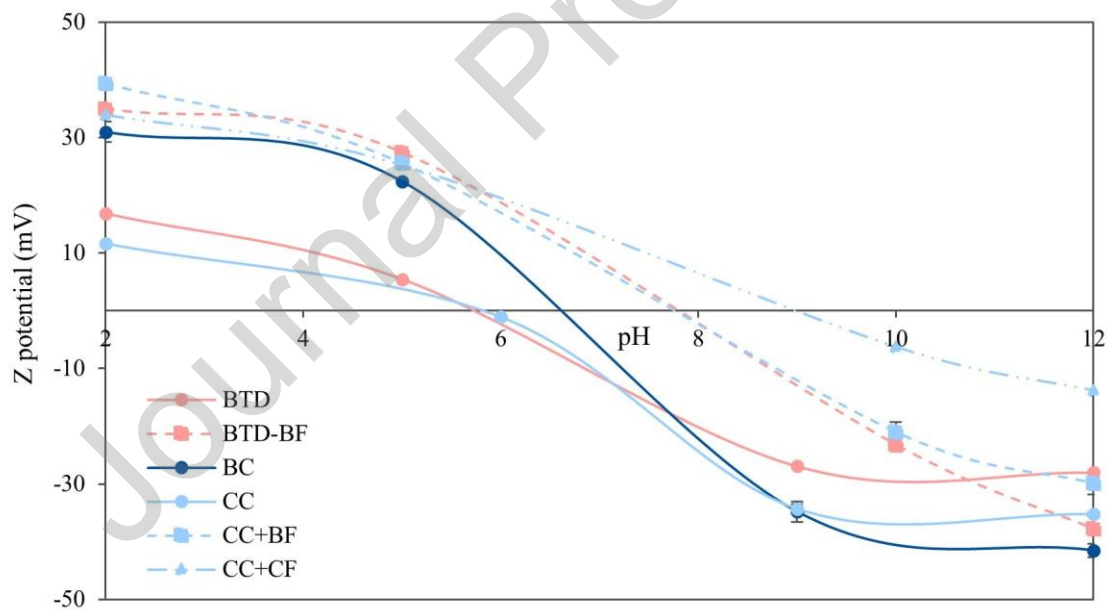


Figure 4. Z potential as function of pH (2-12) for the different MNPs samples synthesized by batch thermal decomposition (BTD), batch thermal decomposition followed by batch amino-functionalization (BTD-BF), batch coprecipitation (BC), continuous coprecipitation (CC), continuous coprecipitation followed by batch amino-functionalization (CC-BF) and continuous coprecipitation followed by continuous amino-functionalization (CC-CF).

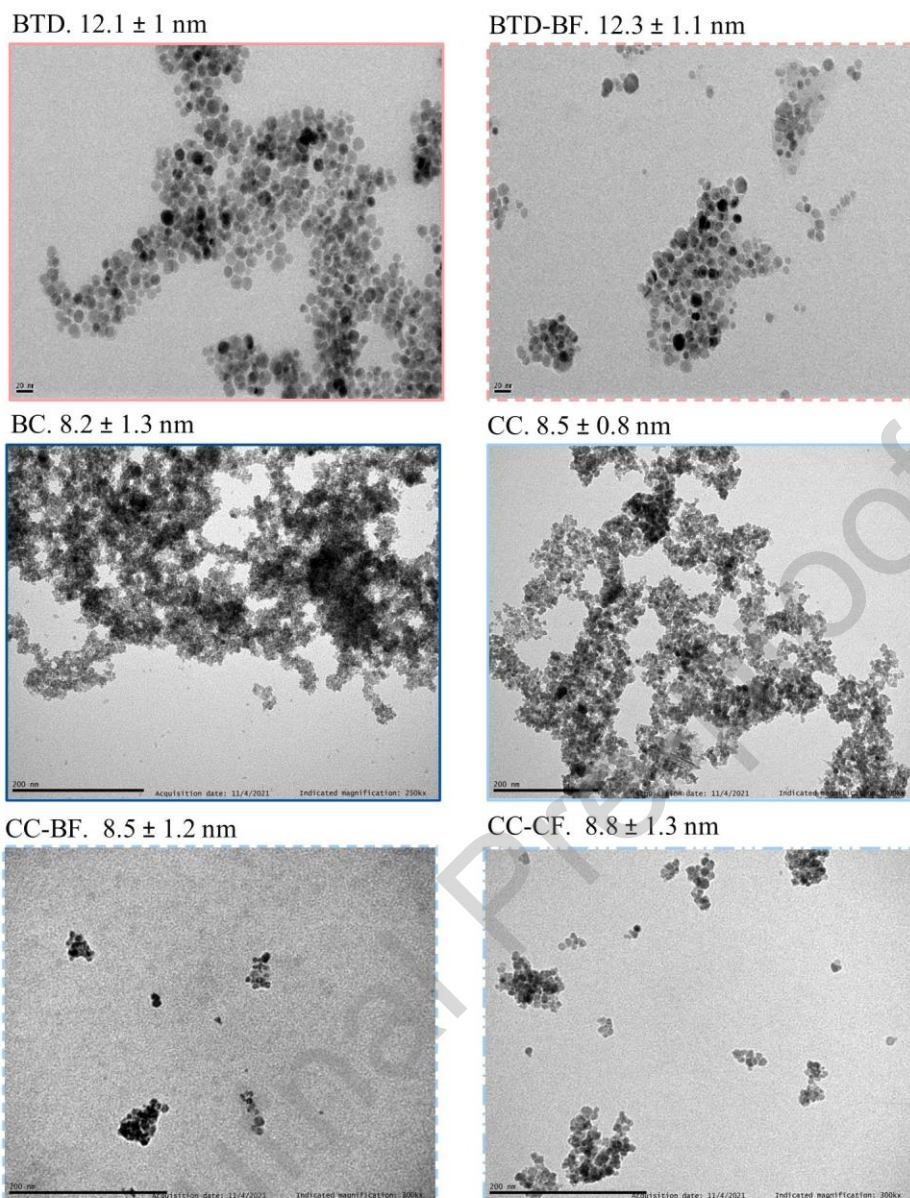


Figure 5. TEM images of the different MNPs samples synthesized by batch thermal decomposition (BTD), batch thermal decomposition followed by batch amino-functionalization (BTD-BF), batch coprecipitation (BC), continuous coprecipitation (CC), continuous coprecipitation followed by batch amino-functionalization (CC-BF) and continuous coprecipitation followed by continuous amino-functionalization (CC-CF). Scale bar for BTD and BTD-BF is 20nm. Scale bar for BC, CC, CC-BF and CC-CF is 200nm.

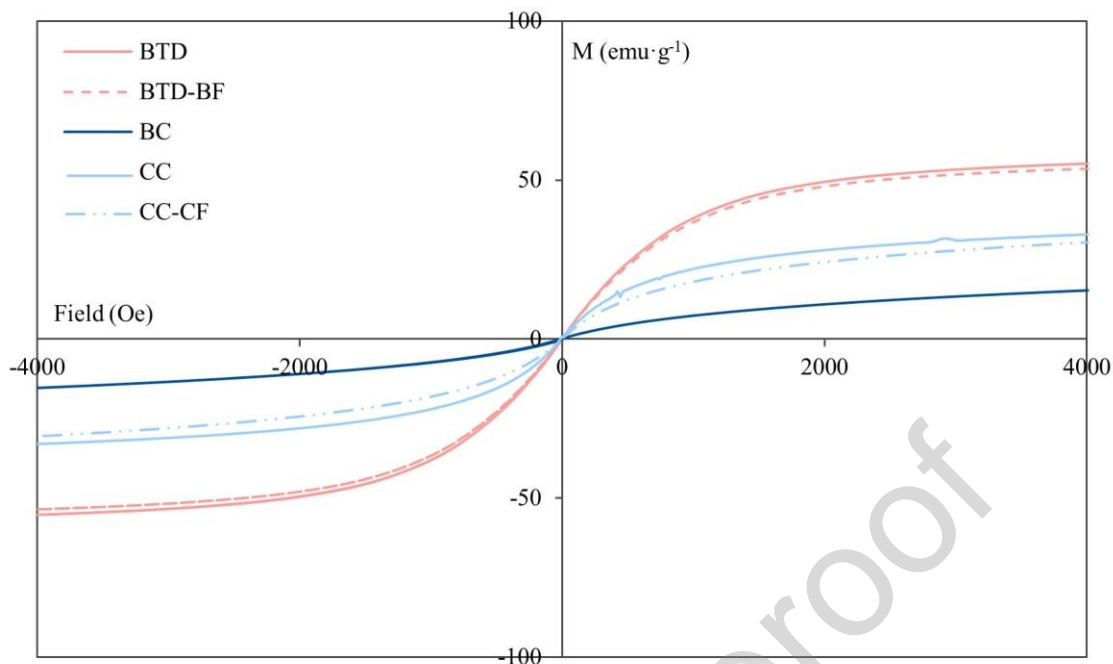


Figure 6. Magnetization curves (27°C) of the different samples synthesized by batch thermal decomposition (BTD), batch thermal decomposition followed by batch amino-functionalization (BTD-BF), batch coprecipitation (BC), continuous coprecipitation (CC) and continuous coprecipitation followed by continuous amino-functionalization (CC-CF).

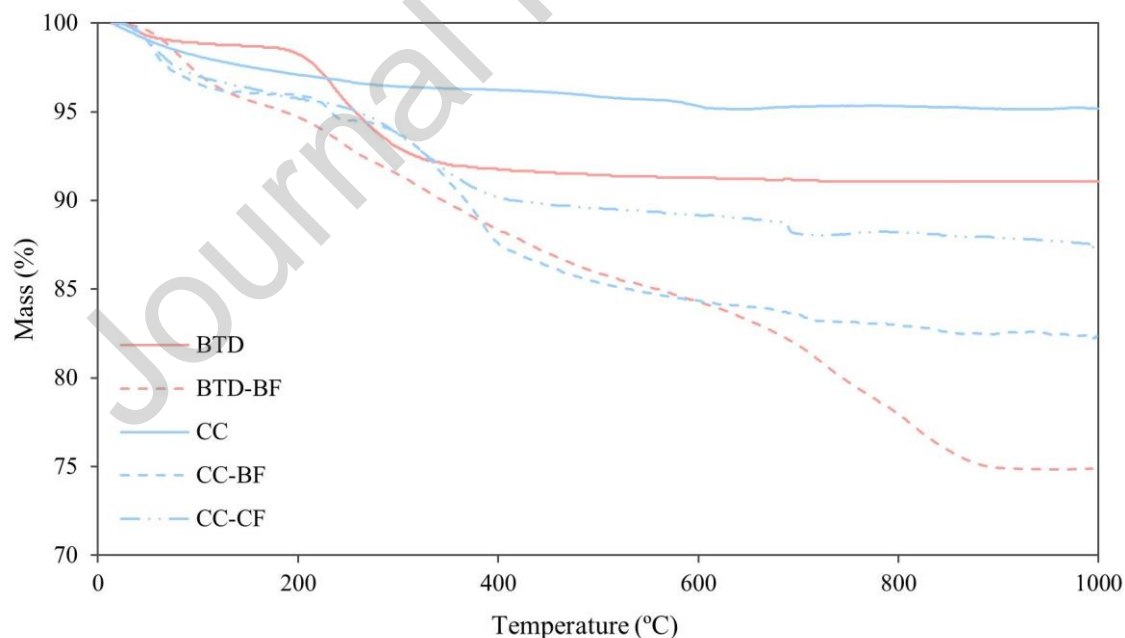


Figure 7. TGA (0 -1000°C) of the different samples synthesized by batch thermal decomposition (BTD), batch thermal decomposition followed by batch amino-functionalization (BTD-BF), batch coprecipitation (BC), continuous coprecipitation (CC), continuous coprecipitation followed by batch amino-functionalization (CC-BF) and continuous coprecipitation followed by continuous amino-functionalization (CC-CF).

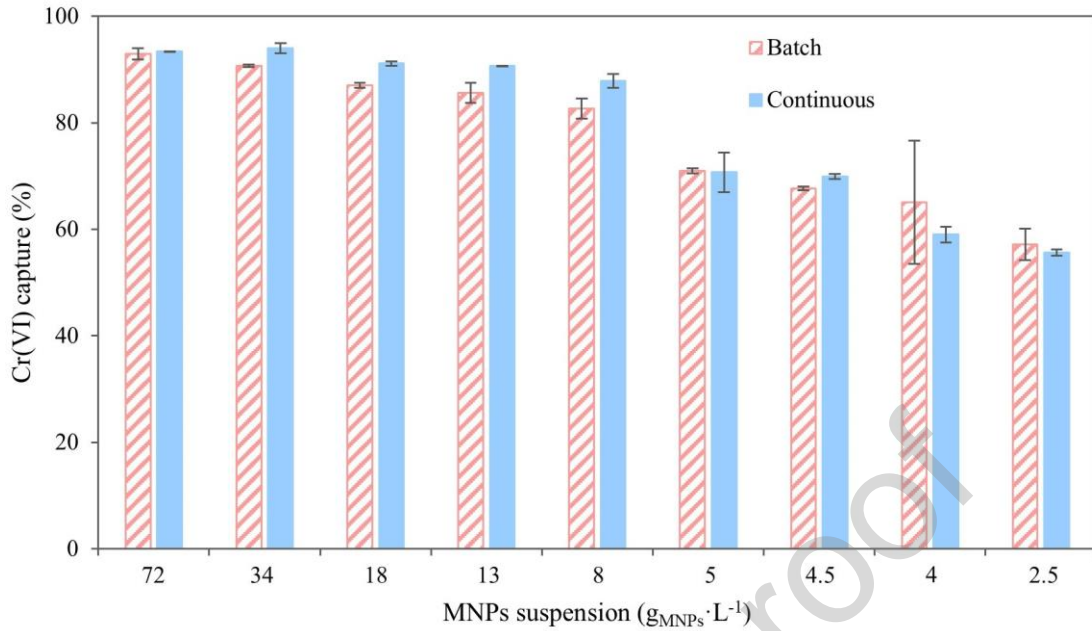


Figure 8. Experimental Cr(VI) capture percentages for batch and continuous mode, contacting a solution with  $23\text{mg}\cdot\text{L}^{-1}$  of Cr(VI) with different BTD-BF suspensions. Batch: 18min contact time. Continuous: 18min residence time and  $78.5\text{L}\cdot\text{min}^{-1}$  flowrate in each inlet.

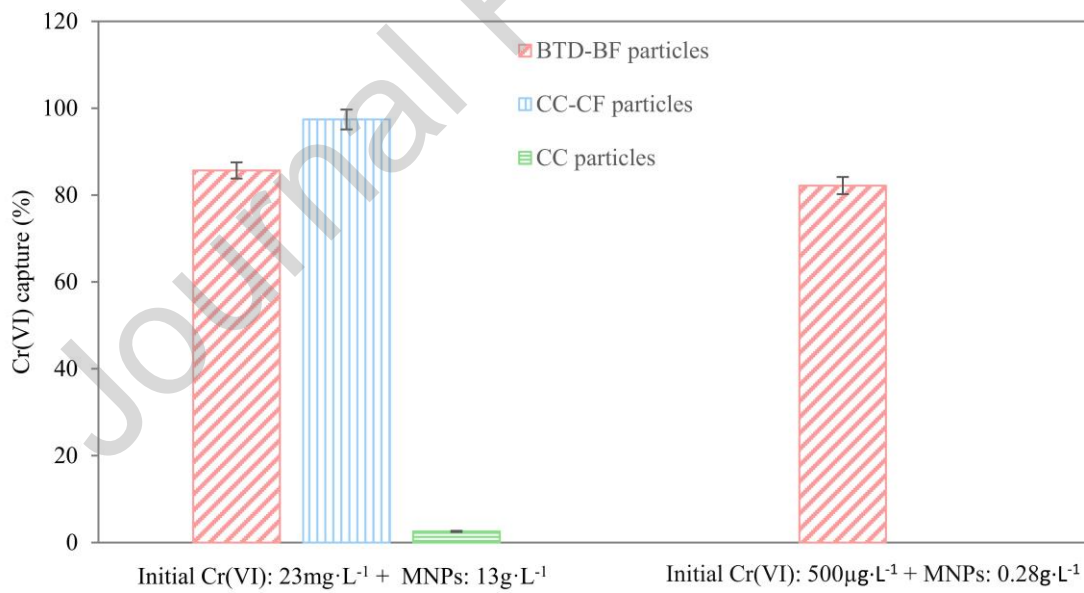


Figure 9. Experimental Cr(VI) capture percentages for batch experiments with i)  $13\text{g}_{\text{MNPs}}\cdot\text{L}^{-1}$  BTD-BF particles and initial Cr(VI) concentration of  $23\text{mg}\cdot\text{L}^{-1}$ , ii)  $13\text{g}_{\text{MNPs}}\cdot\text{L}^{-1}$  CC-CF particles and initial Cr(VI) concentration of  $23\text{mg}\cdot\text{L}^{-1}$ , iii)  $13\text{g}_{\text{MNPs}}\cdot\text{L}^{-1}$  CC particles and initial Cr(VI) concentration of  $23\text{mg}\cdot\text{L}^{-1}$ , and iv)  $0.28\text{g}_{\text{MNPs}}\cdot\text{L}^{-1}$  BTD-BF particles and initial Cr(VI) concentration of  $500\mu\text{g}\cdot\text{L}^{-1}$ . Conditions for all experiments: 18min contact time.

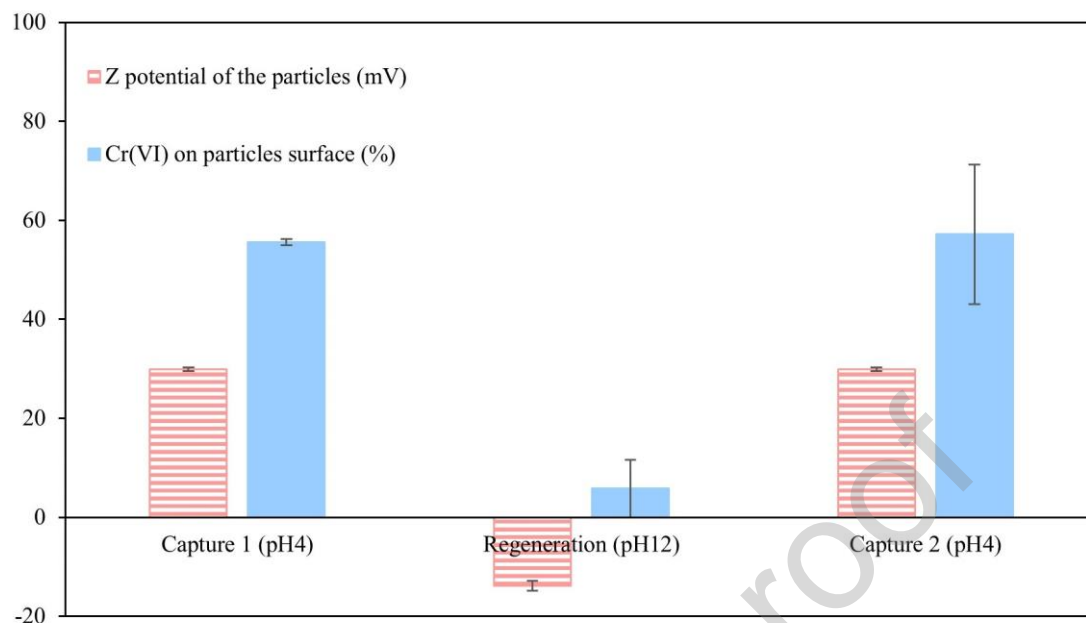


Figure 10. Z potential of the particles (mV), and Cr(VI) on particles surface (%) after the first Cr(VI) capture experiment, the MNPs regeneration with NaOH and the second Cr(VI) capture experiment. Conditions: BTD-BF suspension:  $2.5\text{g}_{\text{MNPs}}\cdot\text{L}^{-1}$ ; residence time: 18 minutes capture and 9 minutes regeneration; Flow rate:  $78.5\mu\text{L}/\text{min}$  for Cr(VI) and MNPs inlet and  $157\mu\text{L}/\text{min}$  for NaOH inlet.

Table 1. MNPs synthesis and functionalization approaches applied in this study

		SYNTHESIS		
		Batch thermal decomposition	Batch coprecipitation	Continuous coprecipitation
FUNCTIONALIZATION	No functionalization	BTD	BC	CC
	Batch functionalization	BTD-BF	-	CC-BF
	Continuous functionalization	-	-	CC-CF

Table 2. Parameters of MNPs used to calculate the degree of functionalization

	BTD-BF	CC-BF	CC-CF
<b>MNPs Diameter (nm)</b>	12.1±1.1	8.5±0.8	8.5±0.8
<b>MNPs Area (nm<sup>2</sup>)</b>	463 ± 76	229 ± 43	229 ± 43
<b>MNPs Volume (nm<sup>3</sup>)</b>	947 ± 231	330 ± 91	330 ± 91
<b>Magnetite density (g·nm<sup>-3</sup>)</b>	5.2·10 <sup>-21</sup>	5.2·10 <sup>-21</sup>	5.2·10 <sup>-21</sup>
<b>Aminoalcoxisilane molecular weight (g·mol<sup>-1</sup>)</b>	222	222	222
<b>Aminoalcoxisilane groups losses (%)</b>	18.1 ± 1.6	12.4 ± 6.4	8.2 ± 0.1
<b>σTGA (molecules<sub>amino</sub>·nm<sup>-2</sup><sub>MNPs</sub>)</b>	6.4 ± 0.6	3.0 ± 1.7	1.8 ± 0.02
<b>MNPs BET area (m<sup>2</sup>·g<sup>-1</sup>)</b>	15.8 ± 0.04	141 ± 0.3	141 ± 0.3
<b>FD (mol<sub>amino</sub>·g<sup>-1</sup><sub>MNPs</sub>)</b>	1.7·10 <sup>-4</sup> ± 1.7·10 <sup>-5</sup>	7·10 <sup>-4</sup> ± 4·10 <sup>-4</sup>	4.2·10 <sup>-4</sup> ± 5.6·10 <sup>-6</sup>

Table 3. Comparison between the Initial conditions and equilibrium parameters of this study and other works with commercial ion exchange technologies.

Technology (size in μm)	Functional group R	Initial Cr (mg·L <sup>-1</sup> )	pH	T (K)	Equilibrium constant (-)	Exchange capacity (meq <sub>Cr(VI)</sub> ·g <sup>-1</sup> <sub>MNPs</sub> )	Ref
BTD-BF MNPs (0.012)	Primary & secondary amine	23	3.4-6 <sup>a</sup>	297	1.51	0.60 <sup>c</sup>	This study

CC-CF MNPs (0.009)	Primary & secondary amine	23	3.4-6 <sup>a</sup>	297	1.51	1.44 <sup>c</sup>	This study
Lewatit MP62 (310-1250)	Tertiary amine	100	5 <sup>b</sup>	298	220	1.67 <sup>d</sup>	[55]
Lewatit M610 (300-1200)	Tertiary amine	100	5 <sup>b</sup>	298	54.44	3.70 <sup>d</sup>	[55]
Lewatit MP64 (590)	Quaternary amine	13.5-409	2 <sup>b</sup>	297	44.90	2.66 <sup>c</sup>	[10]
Lewatit MP 64 (590)	Quaternary amine	52	5 <sup>b</sup>	298	3.41	1.25 <sup>d</sup>	[57]
Lewatit MP500 (630)	Quaternary amine	52	5 <sup>b</sup>	298	3.27	1.32 <sup>d</sup>	[57]

a= final pH; b= initial pH.

c=Maximum Cr(VI) exchange capacity calculated from experimental data; d=Minimum value reported by the manufacturer without specifying the experimental conditions;

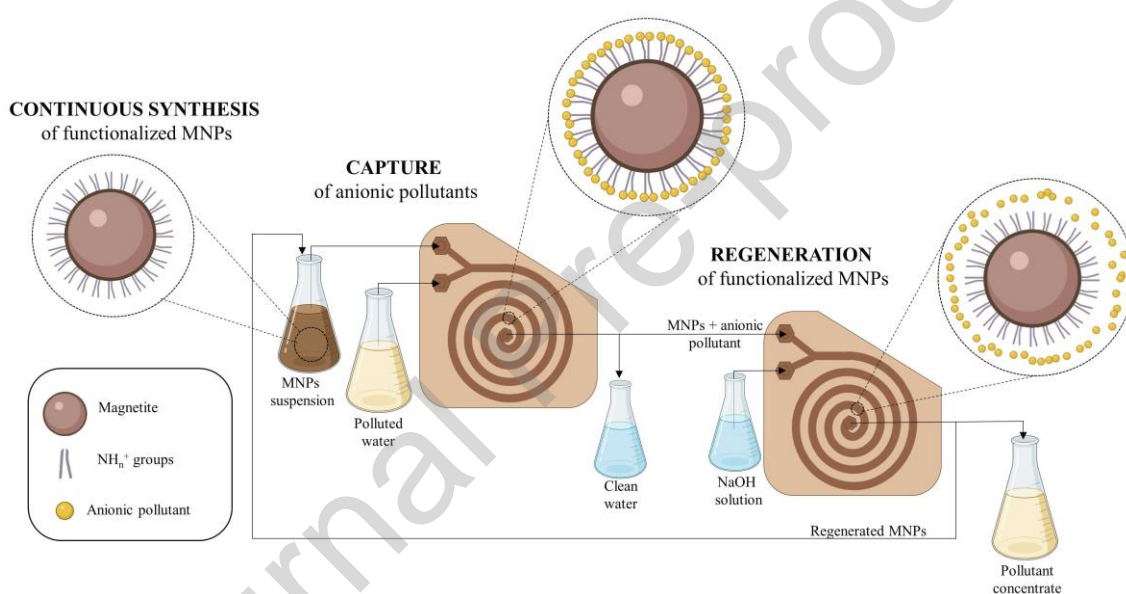
## CRediT authorship contribution statement

**Belén García:** Methodology, Investigation, Data curation, Writing –original draft, **Eugenio Bringas:** Conceptualization, Writing – review & editing, Resources, Supervision, **Inmaculada Ortiz:** Conceptualization, Writing – review & editing, Resources, Supervision, Project administration, Funding acquisition.

## Declaration of Competing Interest

The authors declare that they have no known competing financial interests or personal relationships that could have appeared to influence the work reported in this paper.

## Graphical abstract



## Highlights

- A robust microfluidic system is proposed for the continuous, rapid and effective testing of selective capture agents of aqueous pollutants.
- Amino-functionalized MNPs have been obtained following a novel continuous synthesis that facilitated the control of the particles properties.
- Continuously synthesized MNPs have been used for the rapid and selective capture of Cr(VI), as representative case study, with good results in terms of capture efficiency.
- The easy regeneration of the loaded MNPs and their successful reuse have been proven.